

# StereoCrafter-Zero: Zero-Shot Stereo Video Generation with Noisy Restart

Jian Shi      Qian Wang      Zhenyu Li      Peter Wonka  
 King Abdullah University of Science and Technology, Thuwal, Saudi Arabia  
 {jian.shi, qian.wang, zhenyu.li.1, peter.wonka}@kaust.edu.sa

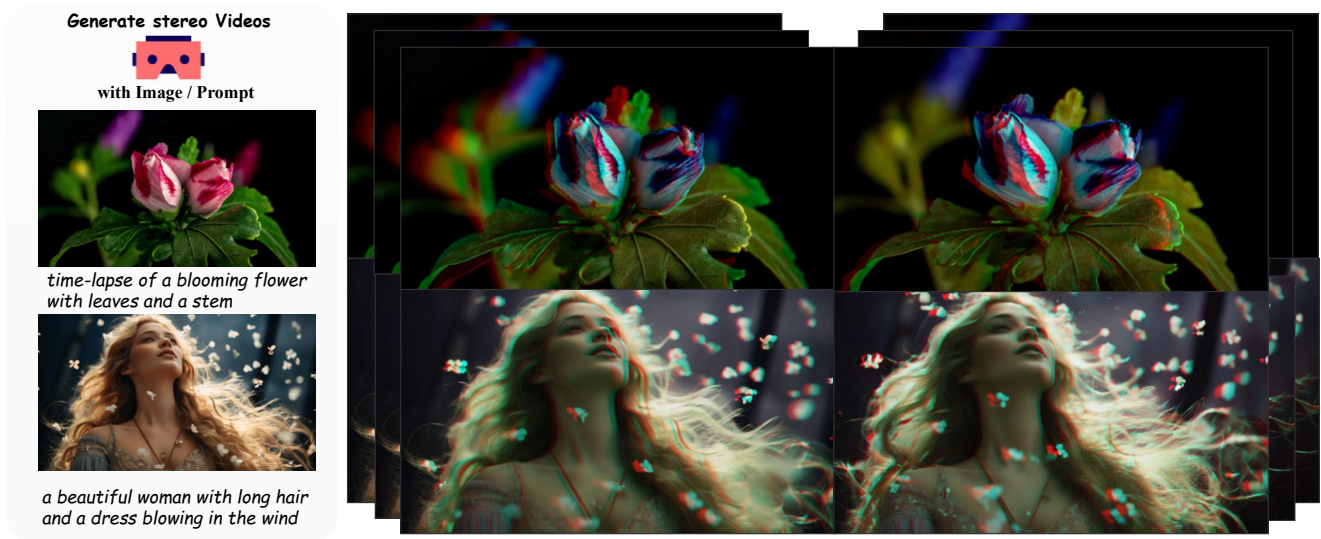


Figure 1. Our method performs stereo video generation with only a single image and a prompt as input. We show anaglyph for best showing the stereoscopic effects.

## Abstract

Generating high-quality stereo videos that mimic human binocular vision requires maintaining consistent depth perception and temporal coherence across frames. While diffusion models have advanced image and video synthesis, generating high-quality stereo videos remains challenging due to the difficulty of maintaining consistent temporal and spatial coherence between left and right views. We introduce StereoCrafter-Zero, a novel framework for zero-shot stereo video generation that leverages video diffusion priors without the need for paired training data. Key innovations include a noisy restart strategy to initialize stereo-aware latents and an iterative refinement process that progressively harmonizes the latent space, addressing issues like temporal flickering and view inconsistencies. Comprehensive evaluations, including quantitative metrics and user studies, demonstrate that StereoCrafter-Zero produces high-quality stereo videos with improved depth consistency and temporal smoothness, even when depth estimations are imperfect. Our framework is robust and adaptable across various diffusion models, setting a new benchmark for zero-

shot stereo video generation and enabling more immersive visual experiences. Our code can be found in <https://github.com/shijianjian/StereoCrafter-Zero>

## 1. Introduction

There is a renewed interest in stereo images and videos due to the recent release of new hardware for head-mounted displays. Stereo image conversion aims to reconstruct stereo pairs from single images. Inconsistent depth information can lead to visual artifacts and a lack of coherence between frames, undermining the immersive experience that stereo videos are intended to provide. Previous works [30, 33, 37, 40, 41] have significantly advanced the ability to generate left and right views that maintain depth consistency and realistic parallax effects. Building upon these foundations, recent studies have extended stereo conversion techniques to video, emphasizing the importance of temporal consistency to produce smooth and coherent stereo video sequences [32, 50]. Concurrently, diffusion

models have emerged as a powerful paradigm for generative tasks, demonstrating remarkable proficiency in capturing complex data distributions and generating high-fidelity images and videos [13, 29, 31]. Notably, StereoDiffusion [38] presented a zero-shot approach that leveraged diffusion models to generate stereo images, showcasing the potential of creating stereo content with generative models without training. In this work, we explore a relatively unexplored field of stereo video generation with diffusion models in a zero-shot manner without significant computational requirements.

Stereo video generation presents unique challenges that differentiate it from single-image stereo. Temporal flickering and view inconsistencies between the left and right views are common issues that degrade the user experience. Therefore, ensuring temporal coherence across frames when extending these methods to video remains a significant challenge, which requires meticulous handling of depth cues to ensure realistic parallax effects and maintaining temporal-consistent depth perception across both left and right views [3]. Notably, recent progress in video depth estimation models improves the temporal consistency by accurately capturing and maintaining depth information across video frames [16, 19, 24]. However, the challenge lies in the nuanced interplay between depth consistency and temporal coherence within the context of diffusion-based stereo video generation. To be specific, maintaining consistency not only between consecutive frames (temporal) but also between the left and right views within each frame (inter-view) is essential. Current video generation models primarily focus on overall visual fidelity and temporal smoothness without explicitly enforcing depth consistency between the left and right views across consecutive frames. Existing methods lack mechanisms to dynamically adapt depth information within the diffusion process to account for scene dynamics for stereo video generation.

Addressing these challenges, we introduce **StereoCrafter-Zero**, a novel framework for zero-shot stereo video generation that leverages video diffusion priors to generate high-quality stereo videos without the need for paired training data. Instead of performing the stereo conversion on the video level, we improve and refine the consistency within the latent features of a video diffusion model. Our approach seamlessly integrates advanced video depth estimation into the diffusion-based synthesis process, ensuring depth consistency and temporal coherence. We carry out quantitative and qualitative studies that demonstrate the effectiveness of our method, including a user study. Our main contributions are as follows:

- we introduce **StereoCrafter-Zero**, a novel approach for zero-shot stereo video generation that can be adapted to various diffusion frameworks without the need for paired training data.

- To enhance the latent consistency, we utilize a *noisy restart* strategy to obtain stereo-aware initial latents. Subsequently, an *iterative refinement* process systematically injects controlled noise into the diffusion process, progressively improving the harmony of the latent space.
- We present comprehensive statistical evaluation and user studies, demonstrating our method can generate high-quality stereo videos.

## 2. Related Works

### 2.1. Video Generation

Diffusion models have achieved great success in text-to-image generation [2, 12, 31]. Recently, diffusion models have been widely adopted in the video domain to produce high-quality videos given text prompts or images as input [4, 14, 15, 28, 42, 43]. Stable Video Diffusion [4] collected and curated a large-scale video dataset to enable video generation with competitive performance. DynamiCrafter [42] proposed to use dual-stream image injection to incorporate images as guidance and can animate input images complemented with text prompts. These models form the foundation of our proposed method for stereo video generation.

However, despite these advances, generating stereo video with synchronized left and right views remains a challenge. Existing methods fail to account for the stereo disparity between views and often suffer from temporal flickering, especially in dynamic scenes.

### 2.2. Novel-View Synthesis

Novel-view synthesis aims to generate images rendered under a novel target camera pose from given source images. Recent novel-view synthesis works such as [21, 22, 35, 36, 45, 46] may achieve a similar goal to create a stereo pair of a given scene, but they require scene-specific optimization which is not suitable to apply on video data. Another branch of works [10, 34, 48] uses depth-warping to synthesize novel views and refines the warped images. These approaches may suffer from artifacts in the inpainted regions. More importantly, handling video-based novel view synthesis may additionally require temporal consistency. CVD [20] utilized a cross-video synchronization module to directly generate multi-view videos given a target camera trajectory. Another line of work [1, 44, 47] explicitly constructed 3D scenes along with temporal changes. Although they can generate novel videos, the domain is limited to simple object-centric scenes and lower visual quality. It still remains a challenge to generate novel-view videos with complex visual content.

### 2.3. Stereo Content Generation

Stereo content generation has evolved significantly from traditional disparity estimation and view synthesis methods

to advanced deep learning techniques that enhance depth accuracy and visual realism. Early approaches utilized neural networks and generative networks to create stereo image pairs by predicting disparity maps and synthesizing corresponding views [37, 41]. Recent advancements have extended these techniques to video, addressing temporal coherence to ensure smooth and immersive stereo video sequences [32, 49, 50]. Concurrently, diffusion models have been successfully adapted for stereo image generation, enabling zero-shot synthesis [38]. However, zero-shot generative models for stereo video are still under exploration, particularly in ensuring both spatial depth fidelity and temporal consistency across frames. A concurrent work [11] proposes a *frame matrix* by placing multiple camera views and warps the latent on every DDIM sampling step. In contrast, our method can generate new viewpoints without the need to perform warping at every step, which can highly reduce the computational cost.

### 3. Preliminaries

**Image Warping for Stereo View Synthesis** Generating a stereo pair of a single input image includes warping the image based on a disparity map. The disparity map  $d$  can be computed using the depth map of the image:

$$d(x, y) = \frac{f \cdot B}{I_{depth}(x, y)}, \quad (1)$$

where  $f$  is the focal length,  $B$  is an adjustable baseline distance, and  $I_{depth}(x, y)$  is the depth value for a pixel at the location  $(x, y)$ . With the disparity map, the right-view image can be obtained by warping the original 2D image with:

$$I_{right}(x - d(x, y), y) = I(x, y). \quad (2)$$

This shift creates a horizontal parallax, mimicking the viewpoint difference. However, the warping operation requires a high precision of the depth map and can introduce artifacts and misalignments. Due to occlusions, some pixels in the right view may not have a corresponding pixel in the original image. Previous works [25, 39, 50] applied inpainting to handle the occluded and disoccluded areas.

**Stereo Pair Generation with Diffusion Models.** Recent works such as [38] propose to warp the latent space of an image diffusion model. This can be achieved since the early-stage sampling in diffusion models involves low-frequency signals that primarily define the contours of the generated image. When the step  $t$  is large, high-frequency signals in the later stage sampling refine the image details. Formally, the generative process for each DDIM step can be described as follows:

$$x_{t-1} = \sqrt{\alpha_{t-1}} \left( \frac{x_t - \sqrt{1 - \alpha_t} \epsilon_\theta^t(x_t)}{\sqrt{\alpha_t}} \right) + \sqrt{1 - \alpha_{t-1} - \sigma_t^2 \epsilon_\theta^2(x_t)} + \sigma_t \epsilon_t, \quad (3)$$

where  $\epsilon_t$  is noise following a standard Gaussian distribution  $\mathcal{N}(0, I)$ , independent of  $x_t$ , and  $\alpha_t$  controls the noise scale at step  $t$  with  $\alpha_0 := 1$ . As the only randomness during the diffusion process, we duplicate the  $\epsilon$  for different views by default in our work. Meanwhile, as demonstrated in Secs. 4.1 and 5, we found the noise level  $\epsilon$  plays an important role in creating stereoscopic effects.

**Cross-View Attention** To enhance multi-view consistency, many works [7–9, 17, 18, 26, 27, 38] modify the diffusion model’s attention mechanism by replacing the query, key, and value pairs, ensuring coherent generation across different views. In this work, we allow the left view’s query (Q) to attend directly to the right view’s key (K) and value (V). This mechanism promotes stronger alignment and coherence across views by sharing essential spatial and contextual information. Let  $Q_L, K_L, V_L$  and  $Q_R, K_R, V_R$  represent the query, key, and value matrices for the left view and right view, respectively. To align the right view with the left view’s features, we use  $Q_L$  (from the left view) to attend to  $K_R$  and  $V_R$  (from the right view). Mathematically, the right view feature  $F_{R \rightarrow L}$  can be expressed as:

$$F_{R \rightarrow L} = \text{softmax} \left( \frac{Q_L K_R^\top}{\sqrt{d}} \right) \cdot V_R. \quad (4)$$

### 4. Method

In this section, we describe the *StereoCrafter-Zero* framework for zero-shot stereo video generation, which leverages video diffusion priors to generate stereo videos. Let  $\mathbf{X} = \{x_T, x_{T-1}, \dots, x_0\}$  denote the DDIM latent sequence from a video diffusion model with  $T$  diffusion steps (e.g.,  $T = 50$ ). Each latent  $x_t \in \mathbb{R}^{B \times C \times T \times H \times W}$  is a five-dimensional tensor representing a batch of video frames, where  $B$  is the batch size,  $C$  is the number of channels,  $T$  is the temporal dimension (number of frames), and  $H$  and  $W$  are the spatial height and width, respectively. By decoding  $x_0$ , we obtain a video sequence  $V \in \mathbb{R}^{B \times 3 \times T \times H' \times W'}$ , where  $H'$  and  $W'$  are the corresponding height and width for the decoded videos. To understand the scene’s geometry and enable accurate latent warping, we generate video depth maps  $\mathbf{D} \in \mathbb{R}^{B \times T \times H' \times W'}$ , that provides per-pixel and temporal-consistent depth information. The latent representations are then warped to achieve stereo consistency and account for parallax effects. Let  $\Delta$  denote the disparity map that is computed by Eq. (1), which represents the horizontal shift between the left and right stereo views, then we can apply the warp operation  $\mathbf{W}(x, \Delta)$  using Eq. (2), resulting in  $x_t^{\text{warp}} = \mathbf{W}(x_t, \Delta)$ . We provide an efficient implementation of the warping algorithm, described in our *supplementary material*. This warping aligns the latent representations to reflect depth-induced disparities, essential for generating realistic stereo views. The warping process introduces blank regions  $x^{\text{blank}} \in \mathbb{R}^{B \times C \times T \times H \times W}$  in the

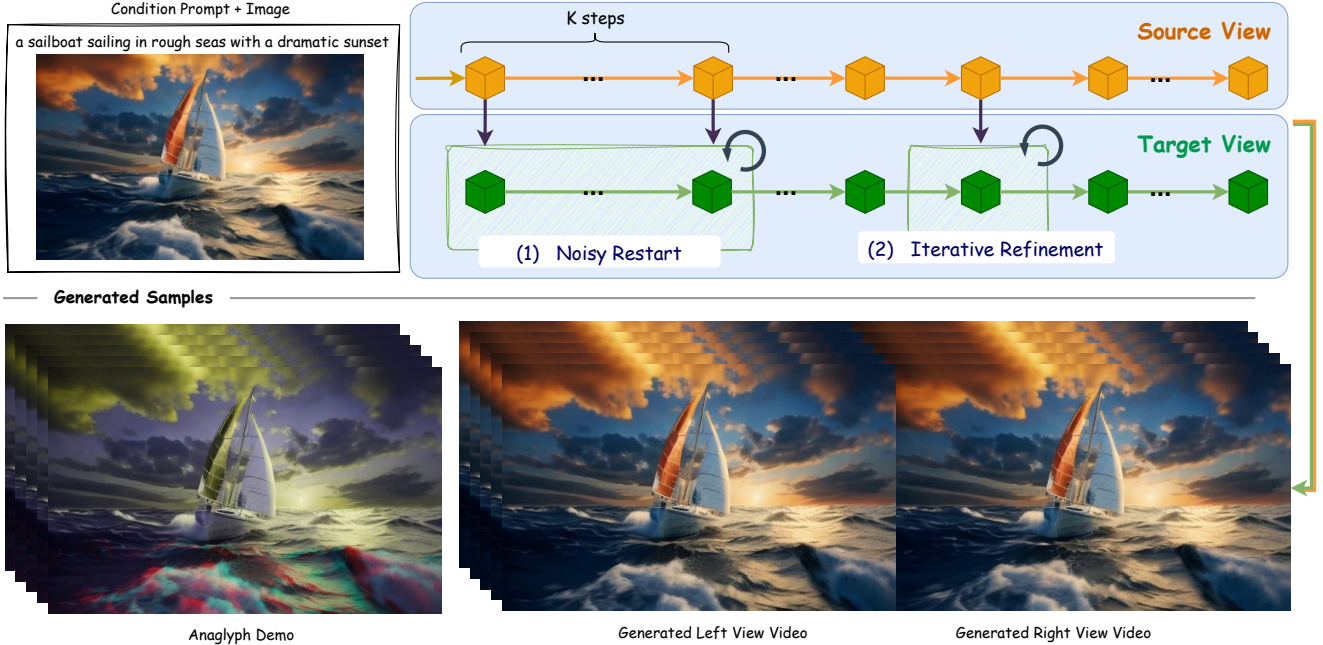


Figure 2. An overview of the *StereoCrafter-Zero* pipeline. Top: our method is based on the techniques of 1) noisy restart that is used to obtain a robust initial latent ( Sec. 4.1) and 2) iterative refinement that refines the latent ( Sec. 4.2) of a sampling step. Bottom: we show that we can generate both the left view and right view from the conditioning image and the text prompt that can create a strong stereoscopic effect.

warped latents due to occlusions or disocclusions:

$$x_t^{blank} = \begin{cases} 1 & \text{if } x_t^{warp} \text{ is undefined,} \\ 0 & \text{otherwise.} \end{cases} \quad (5)$$

With the aid of a disparity map, each latent feature can be decoupled to  $x_t^{blank}$  and  $x_t^{warp}$ , and the consistency of those two latent parts is critical to creating meaningful and harmonized outputs for each individual view with correct depth cues. Clearly,  $\epsilon_t$  is the only randomness during the diffusion process referring back to Eq. (3). We, therefore, focus on refining the latent features by iteratively injecting  $\epsilon_t$  in the diffusion process.

The main contribution of our paper is to improve consistency between  $x_t^{blank}$  and  $x_t^{warp}$ . Briefly, we first use noisy restart (Sec. 4.1) to initialize a reasonable  $x^{blank}$ , then use an iterative refinement (Sec. 4.2) to improve the consistency between  $x^{warp}$  and  $x^{blank}$ .

#### 4.1. Noisy Restart

The noisy restart mechanism is implemented over  $K$  diffusion steps for  $N$  iterations. We denote the  $K$  diffusion step as  $\{x_t\}_{t=0}^K$ , where  $x_t$  represents the latent state at step  $t$ . Note that  $K$  can be a set of discrete timesteps, while we use  $K = \{0, \dots, 5\}$ . The general idea of the noisy start is to introduce random noise to the filling latent to prevent structural repetition and promote smooth transitions. So that the

first iteration generates  $K$  filling latents for each diffusion step, while the future iterations will keep iterating on the obtained  $K$  latents. Refer to Eq. (3), a random noise  $\epsilon_t$  is introduced in each sampling step. This randomness of  $\epsilon_t$  may break the consistency between multiple iterations if each iteration uses different random noises. In order to avoid it in the noisy restart stage, prior to the start of each diffusion sampling sequence, we initialize fixed noise tensors  $\epsilon'_t$ , then set the same random seed for each iteration. This operation keeps the same random generator status across multiple iterations, which ensures the noise injection is purely controlled by  $\epsilon'_t$  and  $\alpha_t$  in Eq. (6). Meanwhile, such a controlled approach provides structural stability throughout the generation process, ensuring consistent low-frequency noise that preserves major features across frames. We showcase the effectiveness of this method in Sec. 5.

In our work, we set a total of  $L = 7$  iterations, and the first iteration directly uses the left-view latents as the filling latents. The noise is injected into the latent state  $x_{t+1}$  with a weighted addition, balancing the influence of the existing latent and the injected noise. The update equation for  $x_{t-1}$  becomes:

$$x_{t-1} = x_t \cdot (1 - \alpha_t) + \sigma_t \epsilon'_t \alpha_t \quad (6)$$

where  $\sigma_t$  is the noise magnitude for each timestep, scaling the impact of injected noise, and we use  $\alpha_t$  as the balancing

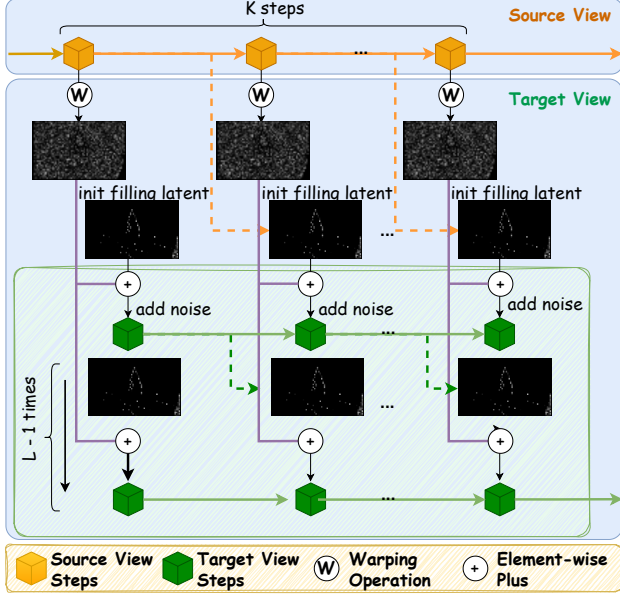


Figure 3. A visualization of the noisy start strategy. At each selected noisy restart step, we replace the target view sampling step with the warped source view, then we fill the occlusion and disocclusion area with the non-warped source view latent. Prior to the sampling, we add additional noise to the latent space. In the next iteration, we update the latents with the value from the previous iteration while keeping the non-occluded areas untouched.

coefficient, controlling the mix between the latent state and the noise.

**Abrupt Border Handling** Direct warping of the right view can result in blank regions along the right border. These blank areas may create irrelevant or distracting content in the border regions during the iterative process. A border mask,  $M_{\text{border}}$ , is created by a heuristic function to select the border areas. We then inpaint the border with the corresponding regions in the left view latents,  $L_l$ . The resulting border refined latent  $L_{r,\text{refined}}$  is defined as:

$$L_{r,\text{refined}} = L_r \cdot (1 - M_{\text{border}}) + L_l \cdot M_{\text{border}}. \quad (7)$$

This operation replaces the blank columns in the right view with the content from the left view, ensuring that the border remains visually continuous and free from distracting artifacts. This border-cleaning step enhances the coherence of the generated stereo image, particularly in maintaining consistency at the edges of the views. We present a qualitative evaluation of this technique in Fig. 4.

## 4.2. Iterative Refinement

By having noisy restart implemented, the stereoscopic effects can be significantly enhanced, as shown in Fig. 7. However, since we are yet only modifying the first several sampling steps, the stereo effects can be shaky and unstable

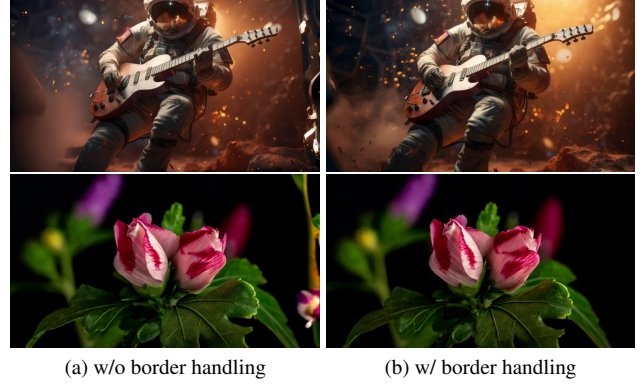


Figure 4. Demonstration of the abrupt border handling. The left column images present abrupt artifacts in the right border, while the right column shows the output with the border properly handled.

across different timeframes. We hereby propose iterative refinement to stabilize the stereo effects for the later sampling stages. The iterative refinement is implemented by repeating the denoising operation at specific sampling steps. At these sampling steps, the model performs multiple iterations to progressively enhance the latent representation. This mechanism enables the model to focus on refining details and correcting errors introduced by the warping operation and earlier steps.

The iterative refinement process is encapsulated in a loop that performs key operations for each propagation step  $j$  within the total number of refinement iterations. Each iteration produces the predicted clean latent  $\hat{x}_0^j$ , scaling factors  $\sqrt{\alpha^j}$ , directional term  $d^j$ , noise  $\epsilon^j$ , and the latent  $x_t^j$  for the next iteration. Starting from the second iteration  $j > 1$ , we update the filling area with the following equation:

$$\hat{x}_0^j = \begin{cases} \hat{x}_0^j * \sqrt{\alpha_t} + \hat{x}_0^{j-1} * (1 - \sqrt{\alpha_t}) & \text{if } x_t^{\text{blank}} = 1, \\ \hat{x}_0^{j-1} & \text{otherwise.} \end{cases} \quad (8)$$

Then the latent is reconstructed by combining the normalized prediction with the directional term and noise:

$$\hat{x}_t = \sqrt{\alpha} \hat{x}_0^j + d_{xt} + \epsilon. \quad (9)$$

Since the latents need to go through the same diffusion denoising process multiple times, we first make sure the predicted latent  $\hat{x}_t$  can maintain statistical consistency across iterations. A scaling factor  $s$  is used to adjust the scale of the latent to the proper scale for its corresponding sampling step. It is computed as:

$$\sigma_t = \sigma(t), \quad \sigma_{t-1} = \sigma(t-1), \quad s = \frac{\sigma_t}{\sigma_{t-1}},$$

where  $\sigma(t)$  denotes the noise level at diffusion step  $t$ . We then simply rescale the latent with  $\hat{x}_t = x_t \times s$ . This scaling

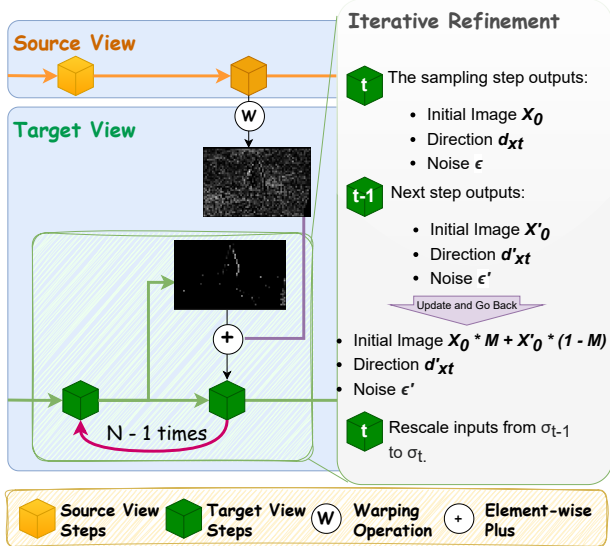


Figure 5. A visualization of iterative refinement. This operation keeps iteratively updating the occluded area within the predicted  $x_0$ . The first iteration proceeds with the normal sampling process, while starting the second iteration, a new predicted latent will be computed and rescaled prior to the next iteration.

adjusts the noise level appropriately, maintaining the stability and convergence of the diffusion process. We update the latent such that we only update the filling latents. Since the later sampling steps are more sensitive to noises, instead of abrupt substitution, we gradually update the filling latents according to  $\alpha_t$ . Lastly, the  $\tilde{x}_t^j$  is taken as the input for the same sampling process again until the total of  $j$  steps.

## 5. Experiments

We present our method based on *DynamiCrafter* [42]. We also evaluated our method with other diffusion-based video generation methods, such as LDM, in our supplementary material. We infer video depth maps with *DepthCrafter* [16]. During the inference, we apply the cross-view attention mechanism on all sampling steps apart from the cross-attention between the latents and the conditions. We use  $L = 7$  for noisy restart from  $t = 0$  to  $t = 5$ . Afterward, we apply warping to update the side-view latent every 5 steps; then each warping step applies iterative refinement. The number of iterations decreases from  $N = 9$  at each refinement step until  $N = 3$ .

**Baseline Methods.** Since there is no direct competitor for zero-shot stereo video generation, we compare our method with different stereo conversion methods such as *ProPainter* (video inpainting), *RoDynRF* (novel-view synthesis), *ImmersePro* (stereo video conversion), and *StereoDiffusion* (stereo image generation). Note that *ImmersePro* is a depth-free method that may create an arbitrary degree of stereo-

scopic effect without the need for a depth map. For benchmarking purposes, we generate 40 video clips with *DynamiCrafter* across various domains such as anime, human, animal, various objects, and imaginary contents. Note that generating one video clip with *RoDynRF* can take around 10 hours with an NVIDIA A100, we therefore neglected it in our benchmark tables but presented a visualization in Fig. 6.

**Quantitative Evaluation** Our evaluation majorly focuses on measuring the consistency between the left view and right view of a generated video. Following previous novel-view rendering methods [5, 6, 20], we report CLIP-based metrics [51] to compute the consistency between 1) the generated view and the text prompt, and 2) the source-view videos and their generated view. As presented in Tab. 3, we achieved the best on both *CLIP-T* and *CLIP-F* that indicates our method improves the semantic and structural consistency between the generated video pair without destroying the content prior.

	ProPainter	ImmersePro	StereoDiffusion	Ours
CLIP-T	29.37	29.58	28.72	<b>29.64</b>
CLIP-F	96.45	96.99	91.09	<b>97.16</b>

Table 1. We measure text-image and semantic consistencies. Our method achieves the best results regarding the matching with the prompt and stereo videos.

**User Study.** We present qualitative evaluations with a Meta Quest 3 headset with 28 users with 5 selected videos. Each user evaluates the quality of the generated videos, as presented in Tab. 2. Our method presents the best overall user rating. Interestingly, though we observe the inpainting-based method may lose fine-grained details, *ProPainter* presents a slightly better stereo effect due to the enforcement of depth cues. Differently, our method pays more attention to the overall harmonization that brings up the overall experience with a slight sacrifice of the stereo effects.

	ProPainter	ImmersePro	StereoDiffusion	Ours
F.Q.	3.93	3.50	3.07	<b>4.29</b>
T.C.	3.93	3.64	2.79	<b>4.07</b>
S.E.	<b>4.00</b>	3.43	3.57	3.92
O.C.	3.93	3.64	3.29	<b>4.29</b>

Table 2. User study statistics of the preference rate for Frame Quality (F.Q.), Temporal Coherence (T.C.), Stereoscopic Effects (S.E.) and overall conformity (O.C.) of the stereo video.

**Qualitative Evaluation** We present visual comparisons against a wide range of similar methods in Fig. 6, and we show stereo videos in our supplementary material. The results show that our method can offer high-quality stereo videos against other methods, in terms of temporal coherence, resolution, and stereo effects. In addition, we show



Figure 6. Comparison with different stereo conversion methods including *ProPainter* (video inpainting), *RoDynRF* (novel-view synthesis), *ImmersePro* (stereo video conversion), and *StereoDiffusion* (stereo image generation). The depth maps for those methods (if needed) are generated by *DepthCrafter*. Those methods mostly fail to handle the border properly. In addition, *ProPainter* can hardly handle the fine details such as rain drops and fire flames, *RoDynRF* can hardly maintain the scene structure correctly, *ImmersePro* may change the brightness of the scene, *StereoDiffusion* may produce more distortion since there are no temporal information constraints. We provide video demonstrations in our supplementary material.



Figure 7. Demonstration of the effectiveness of noisy restart. We present an anaglyph for the best visualization of stereo effects. With higher noisy restart iterations, the strength of stereo effects keeps increasing. The results here are with noisy restart only, without warping in the later stages and iterative refinement.

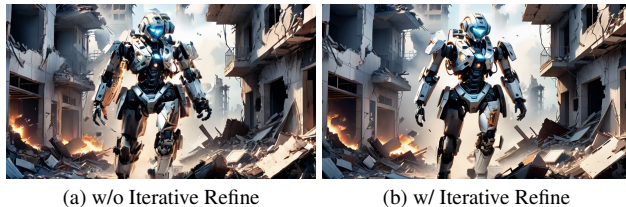


Figure 8. We show the effectiveness of iterative refinement. Without iterative refinement, the filling area after warping in the later sampling stages may be corrupted. With iterative refine, the filling areas are better handled with better consistency.

visualizations of the effectiveness of our proposed modules in Figs. 7 and 8. We strongly recommend readers watch the videos in our supplementary material since the temporal coherence and spatial jittering are hard to see in static figures.

## 6. Discussion and Limitations

We implement our method based on *DynamiCrafter* [42] since it can also be used for longer video generation and generative frame interpolation. We present further demonstrations in our supplementary material. We recommend readers to watch the videos in our supplementary material to get an idea of different methods.

**Imperfect Depth Maps.** Our method takes advantage of the SOTA video depth estimation model, *DepthCrafter* [16]. However, a depth estimation model captures both low-frequency and high-frequency depth changes. When we apply it to the initial sampling steps, the low-frequency depth maps mainly provide the critical information, while the high-frequency depth changes can be noise. Therefore, it may result in lower stability if a video motion of high-frequency information is too strong. We demonstrate such potential behavior in our supplementary material. Meanwhile, we also evaluate the scenario that the depth map itself is imperfect. We simulate such conditions with a disparity propagation method that generates video

depth maps with only a depth image of a single frame and propagates with optical flow. Though a higher precision of video depth estimators is preferred, we found the need for high-quality depth maps can be mitigated by stopping the iterative refinement in the later sampling stages.

**Noise-Powered Latent Refinement.** Repaint [23] first proposed to perturb unmasked regions with noises for inpainting purposes. Unlike image diffusion models, in our experiment, video diffusion models possess a strong denoising ability that effectively counteracts warping effects within the low-frequency latents in the early-stage sampling. As shown in Fig. 7, a straight-forward warping-and-filling can hardly make any effects. Though the warped areas are unchanged, the stereo effects begin to grow stronger by keeping the filling areas noisy. This observation highlights the importance and sensitivity of the latent space in a video diffusion model. SVG [11] uses a similar approach that iteratively refines the latent space of a diffusion model with DDPM scheduling. Since a DDIM scheduler is used in our work, the fundamental difference is that a finer control of noises is required due to the larger skip of steps. Therefore, our work heavily reused diffusion parameters such as  $\sigma_t$  and  $\alpha_t$  for better controlling the noise level. Ideally, with later steps, a smaller level of noise will be used to avoid abrupt changes in the noise space. In our experiment, we found that the later step latent spaces can be fragile. We, therefore, gradually decrease the number of iterations for performing refinement in the later stages.

## 7. Conclusion

In this work, we introduce *StereoCrafter-Zero*, a novel approach for zero-shot stereo video generation. We introduced *noisy restart* and *iterative refinement* for generating stereo videos that together produce stable stereoscopic effects while maintaining temporal and spatial coherence. We perform statistical and user evaluations, demonstrating the effectiveness and usability of our proposed method.

## References

- [1] Sherwin Bahmani, Ivan Skorokhodov, Victor Rong, Gordon Wetzstein, Leonidas Guibas, Peter Wonka, Sergey Tulyakov, Jeong Joon Park, Andrea Tagliasacchi, and David B. Lindell. 4d-fy: Text-to-4d generation using hybrid score distillation sampling. *IEEE Conference on Computer Vision and Pattern Recognition (CVPR)*, 2024. 2
- [2] Yogesh Balaji, Seungjun Nah, Xun Huang, Arash Vahdat, Jiaming Song, Qinsheng Zhang, Karsten Kreis, Miika Aittala, Timo Aila, Samuli Laine, Bryan Catanzaro, Tero Karras, and Ming-Yu Liu. ediff-i: Text-to-image diffusion models with ensemble of expert denoisers. *arXiv preprint arXiv:2211.01324*, 2022. 2
- [3] Jonathan T Barron and Jovan Popović. Structure-from-motion with oriented points. In *IEEE Transactions on Pattern Analysis and Machine Intelligence*, 2015. 2
- [4] Andreas Blattmann, Tim Dockhorn, Sumith Kulal, Daniel Mendelevitch, Maciej Kilian, Dominik Lorenz, Yam Levi, Zion English, Vikram Voleti, Adam Letts, Varun Jampani, and Robin Rombach. Stable video diffusion: Scaling latent video diffusion models to large datasets, 2023. 2
- [5] Shengqu Cai, Eric Ryan Chan, Songyou Peng, Mohamad Shahbazi, Anton Obukhov, Luc Van Gool, and Gordon Wetzstein. Diffdreamer: Towards consistent unsupervised single-view scene extrapolation with conditional diffusion models. In *Proceedings of the IEEE/CVF International Conference on Computer Vision*, pages 2139–2150, 2023. 6
- [6] Shengqu Cai, Duygu Ceylan, Matheus Gadelha, Chun-Hao Paul Huang, Tuanfeng Yang Wang, and Gordon Wetzstein. Generative rendering: Controllable 4d-guided video generation with 2d diffusion models. In *Proceedings of the IEEE/CVF Conference on Computer Vision and Pattern Recognition*, pages 7611–7620, 2024. 6
- [7] Mingdeng Cao, Xintao Wang, Zhongang Qi, Ying Shan, Xiao-hu Qie, and Yinqiang Zheng. Masactrl: Tuning-free mutual self-attention control for consistent image synthesis and editing. In *Proceedings of the IEEE/CVF International Conference on Computer Vision*, pages 22560–22570, 2023. 3
- [8] Songyan Chen and Jiancheng Huang. Fec: Three finetuning-free methods to enhance consistency for real image editing. In *2023 International Conference on Image Processing, Computer Vision and Machine Learning (ICICML)*, pages 76–87. IEEE, 2023.
- [9] Xi Chen, Lianghua Huang, Yu Liu, Yujun Shen, Deli Zhao, and Hengshuang Zhao. Anydoor: Zero-shot object-level image customization. In *Proceedings of the IEEE/CVF Conference on Computer Vision and Pattern Recognition*, pages 6593–6602, 2024. 3
- [10] Jaeyoung Chung, Suyoung Lee, Hyeongjin Nam, Jaerin Lee, and Kyoung Mu Lee. Luciddreamer: Domain-free generation of 3d gaussian splatting scenes. *arXiv preprint arXiv:2311.13384*, 2023. 2
- [11] Peng Dai, Feitong Tan, Qiangeng Xu, David Futschik, Ruofei Du, Sean Fanella, Xiaojuan Qi, and Yinda Zhang. Svc: 3d stereoscopic video generation via denoising frame matrix. *arXiv preprint arXiv:2407.00367*, 2024. 3, 8
- [12] Patrick Esser, Sumith Kulal, Andreas Blattmann, Rahim Entezari, Jonas Müller, Harry Saini, Yam Levi, Dominik Lorenz, Axel Sauer, Frederic Boesel, Dustin Podell, Tim Dockhorn, Zion English, and Robin Rombach. Scaling rectified flow transformers for high-resolution image synthesis. In *Forty-first International Conference on Machine Learning*, 2024. 2
- [13] Jonathan Ho, Ajay Jain, and Pieter Abbeel. Denoising diffusion probabilistic models. In *Advances in Neural Information Processing Systems*, 2020. 2
- [14] Jonathan Ho, William Chan, Chitwan Saharia, Jay Whang, Ruiqi Gao, Alexey Gritsenko, Diederik P. Kingma, Ben Poole, Mohammad Norouzi, David J. Fleet, and Tim Salimans. Imagen video: High definition video generation with diffusion models, 2022. 2
- [15] Jonathan Ho, Tim Salimans, Alexey Gritsenko, William Chan, Mohammad Norouzi, and David J Fleet. Video diffusion models. In *Advances in Neural Information Processing Systems*, pages 8633–8646. Curran Associates, Inc., 2022. 2
- [16] Wenbo Hu, Xiangjun Gao, Xiaoyu Li, Sijie Zhao, Xiaodong Cun, Yong Zhang, Long Quan, and Ying Shan. Depthcrafter: Generating consistent long depth sequences for open-world videos. *arXiv preprint arXiv:2409.02095*, 2024. 2, 6, 8
- [17] Jiancheng Huang, Yifan Liu, Jin Qin, and Shifeng Chen. Kv inversion: Kv embeddings learning for text-conditioned real image action editing. In *Chinese Conference on Pattern Recognition and Computer Vision (PRCV)*, pages 172–184. Springer, 2023. 3
- [18] Anant Khandelwal. Infusion: Inject and attention fusion for multi concept zero-shot text-based video editing. In *Proceedings of the IEEE/CVF International Conference on Computer Vision*, pages 3017–3026, 2023. 3
- [19] Johannes Kopf, Xuejian Rong, and Jia-Bin Huang. Robust consistent video depth estimation. In *Proceedings of the IEEE/CVF Conference on Computer Vision and Pattern Recognition*, pages 1611–1621, 2021. 2
- [20] Zhengfei Kuang, Shengqu Cai, Hao He, Yinghao Xu, Hongsheng Li, Leonidas Guibas, and Gordon. Wetzstein. Collaborative video diffusion: Consistent multi-video generation with camera control. In *arXiv*, 2024. 2, 6
- [21] Zhengqi Li, Qianqian Wang, Forrester Cole, Richard Tucker, and Noah Snavely. Dynibar: Neural dynamic image-based rendering. In *Proceedings of the IEEE/CVF Conference on Computer Vision and Pattern Recognition (CVPR)*, pages 4273–4284, 2023. 2
- [22] Yu-Lun Liu, Chen Gao, Andreas Meuleman, Hung-Yu Tseng, Ayush Saraf, Changil Kim, Yung-Yu Chuang, Johannes Kopf, and Jia-Bin Huang. Robust dynamic radiance fields. In *Proceedings of the IEEE/CVF Conference on Computer Vision and Pattern Recognition*, 2023. 2
- [23] Andreas Lugmayr, Martin Danelljan, Andres Romero, Fisher Yu, Radu Timofte, and Luc Van Gool. Repaint: Inpainting using denoising diffusion probabilistic models. In *Proceedings of the IEEE/CVF conference on computer vision and pattern recognition*, pages 11461–11471, 2022. 8
- [24] Xuan Luo, Jia-Bin Huang, Richard Szeliski, Kevin Matzen, and Johannes Kopf. Consistent video depth estimation. *ACM Transactions on Graphics (ToG)*, 39(4):71–1, 2020. 2

- [25] Lukas Mehl, Andrés Bruhn, Markus Gross, and Christopher Schroers. Stereo conversion with disparity-aware warping, compositing and inpainting. In *Proceedings of the IEEE/CVF Winter Conference on Applications of Computer Vision*, pages 4260–4269, 2024. 3
- [26] Chong Mou, Xintao Wang, Jiechong Song, Ying Shan, and Jian Zhang. Dragondiffusion: Enabling drag-style manipulation on diffusion models. *arXiv preprint arXiv:2307.02421*, 2023. 3
- [27] Jisu Nam, Heesu Kim, DongJae Lee, Siyoon Jin, Seungryong Kim, and Seunggyu Chang. Dreammatcher: Appearance matching self-attention for semantically-consistent text-to-image personalization. In *Proceedings of the IEEE/CVF Conference on Computer Vision and Pattern Recognition*, pages 8100–8110, 2024. 3
- [28] OpenAI. Video generation models as world simulators. 2
- [29] Aditya Ramesh, Prafulla Dhariwal, Alex Nichol, Casey Chu, and Mark Chen. Hierarchical text-conditional image generation with clip latents. *arXiv preprint arXiv:2204.06125*, 1(2):3, 2022. 2
- [30] Rene Ranftl, Katrin Lasinger, David Hafner, Konrad Schindler, and Vladlen Koltun. Towards robust monocular depth estimation: Mixing datasets for zero-shot cross-dataset transfer. *IEEE Transactions on Pattern Analysis and Machine Intelligence*, 44(3):1623–1637, 2022. 1
- [31] Robin Rombach, Andreas Blattmann, Dominik Lorenz, Patrick Esser, and Björn Ommer. High-resolution image synthesis with latent diffusion models. In *arXiv preprint arXiv:2112.10752*, 2022. 2
- [32] Jian Shi, Zhenyu Li, and Peter Wonka. Immersepro: End-to-end stereo video synthesis via implicit disparity learning. *arXiv preprint arXiv:2410.00262*, 2024. 1, 3
- [33] Meng-Li Shih, Shih-Yang Su, Johannes Kopf, and Jia-Bin Huang. 3d photography using context-aware layered depth inpainting. In *IEEE Conference on Computer Vision and Pattern Recognition (CVPR)*, 2020. 1
- [34] Jaidev Shriram, Alex Trevithick, Lingjie Liu, and Ravi Ramamoorthi. Realmdreamer: Text-driven 3d scene generation with inpainting and depth diffusion. *arXiv preprint arXiv:2404.07199*, 2024. 2
- [35] Jingxiang Sun, Bo Zhang, Ruizhi Shao, Lizhen Wang, Wen Liu, Zhenda Xie, and Yebin Liu. Dreamcraft3d: Hierarchical 3d generation with bootstrapped diffusion prior. *arXiv preprint arXiv:2310.16818*, 2023. 2
- [36] Junshu Tang, Tengfei Wang, Bo Zhang, Ting Zhang, Ran Yi, Lizhuang Ma, and Dong Chen. Make-it-3d: High-fidelity 3d creation from a single image with diffusion prior, 2023. 2
- [37] Chaoyang Wang, Simon Lucey, Federico Perazzi, and Oliver Wang. Web stereo video supervision for depth prediction from dynamic scenes. In *2019 International Conference on 3D Vision (3DV)*, pages 348–357. IEEE, 2019. 1, 3
- [38] Lezhong Wang, Jeppe Revall Frisvad, Mark Bo Jensen, and Siavash Arjomand Bigdeli. Stereodiffusion: Training-free stereo image generation using latent diffusion models. In *Proceedings of the IEEE/CVF Conference on Computer Vision and Pattern Recognition*, pages 7416–7425, 2024. 2, 3
- [39] Jamie Watson, Oisín Mac Aodha, Daniyar Turmukhambetov, Gabriel J. Brostow, and Michael Firman. Learning stereo from single images. In *European Conference on Computer Vision (ECCV)*, 2020. 3
- [40] Jamie Watson, Oisín Mac Aodha, Daniyar Turmukhambetov, Gabriel J Brostow, and Michael Firman. Learning stereo from single images. In *Computer Vision—ECCV 2020: 16th European Conference, Glasgow, UK, August 23–28, 2020, Proceedings, Part I 16*, pages 722–740. Springer, 2020. 1
- [41] Junyuan Xie, Ross Girshick, and Ali Farhadi. Deep3d: Fully automatic 2d-to-3d video conversion with deep convolutional neural networks. In *Computer Vision—ECCV 2016: 14th European Conference, Amsterdam, The Netherlands, October 11–14, 2016, Proceedings, Part IV 14*, pages 842–857. Springer, 2016. 1, 3
- [42] Jinbo Xing, Menghan Xia, Yong Zhang, Haoxin Chen, Wangbo Yu, Hanyuan Liu, Xintao Wang, Tien-Tsin Wong, and Ying Shan. Dynamicrafter: Animating open-domain images with video diffusion priors. *arXiv preprint arXiv:2310.12190*, 2023. 2, 6, 8
- [43] Zhuoyi Yang, Jiayan Teng, Wendi Zheng, Ming Ding, Shiyu Huang, Jiazheng Xu, Yuanming Yang, Wenyi Hong, Xiaohan Zhang, Guanyu Feng, et al. Cogvideox: Text-to-video diffusion models with an expert transformer. *arXiv preprint arXiv:2408.06072*, 2024. 2
- [44] Heng Yu, Chaoyang Wang, Peiye Zhuang, Willi Menapace, Aliaksandr Siarohin, Junli Cao, Laszlo A Jeni, Sergey Tulyakov, and Hsin-Ying Lee. 4real: Towards photorealistic 4d scene generation via video diffusion models, 2024. 2
- [45] Wangbo Yu, Li Yuan, Yan-Pei Cao, Xiangjun Gao, Xiaoyu Li, Wenbo Hu, Long Quan, Ying Shan, and Yonghong Tian. Hifi-123: Towards high-fidelity one image to 3d content generation. *arXiv preprint arXiv:2310.06744*, 2023. 2
- [46] Wangbo Yu, Jinbo Xing, Li Yuan, Wenbo Hu, Xiaoyu Li, Zhipeng Huang, Xiangjun Gao, Tien-Tsin Wong, Ying Shan, and Yonghong Tian. Viewrafter: Taming video diffusion models for high-fidelity novel view synthesis. *arXiv preprint arXiv:2409.02048*, 2024. 2
- [47] Haiyu Zhang, Xinyuan Chen, Yaohui Wang, Xihui Liu, Yunhong Wang, and Yu Qiao. 4diffusion: Multi-view video diffusion model for 4d generation. *arXiv preprint arXiv:2405.20674*, 2024. 2
- [48] Jingbo Zhang, Xiaoyu Li, Ziyu Wan, Can Wang, and Jing Liao. Text2nerf: Text-driven 3d scene generation with neural radiance fields. *IEEE Transactions on Visualization and Computer Graphics*, 2024. 2
- [49] Zheyu Zhang and Ronggang Wang. Temporal3d: 2d-to-3d video conversion network with multi-frame fusion. In *2022 4th International Conference on Advances in Computer Technology, Information Science and Communications (CTISC)*, pages 1–5. IEEE, 2022. 3
- [50] Sijie Zhao, Wenbo Hu, Xiaodong Cun, Yong Zhang, Xiaoyu Li, Zhe Kong, Xiangjun Gao, Muyao Niu, and Ying Shan. Stereocrafter: Diffusion-based generation of long and high-fidelity stereoscopic 3d from monocular videos. *arXiv preprint arXiv:2409.07447*, 2024. 1, 3

[51] SUN Zhengwentai. clip-score: CLIP Score for PyTorch. <https://github.com/taited/clip-score>, 2023. Version 0.1.1. 6

# StereoCrafter-Zero: Zero-Shot Stereo Video Generation with Noisy Restart

## Supplementary Material

### A. An Efficient Warping Algorithm

We present a vectorization technique for efficiently implementing pixel-wise image transformations that involve pixel displacement maps. Traditional implementations of such transformations rely on nested loops to process each pixel individually, which can be computationally intensive and inefficient, especially for high-resolution images or large batches. Our method addresses these inefficiencies by leveraging advanced tensor operations in PyTorch to vectorize the computations while ensuring the correctness of the output, particularly in handling overlapping pixel assignments and maintaining the original assignment order.

**Problem Formulation** Let  $I \in \mathbb{R}^{B \times C \times H \times W}$  be a batch of input images, where  $B$  is the batch size,  $C$  is the number of channels, and  $H$  and  $W$  are the height and width of the images, respectively. Let  $D \in \mathbb{R}^{B \times 1 \times H \times W}$  be the corresponding batch of depth maps or optical flow fields. The goal is to create a derived image  $I'$  by displacing pixels from the input image  $I$  based on the values in  $D$ , scaled by a factor  $s$  and an exponent  $\alpha$ . This transformation can be formalized as:

$$I'_{b,c,h,w'} = I_{b,c,h,w}, \quad \text{where } w' = w + \text{offset}_{b,h,w}, \quad (10)$$

$$\text{offset}_{b,h,w} = (D_{b,0,h,w}^\alpha \times s). \quad (11)$$

The challenge arises when multiple source pixels  $(b, c, h, w)$  map to the same destination pixel  $(b, c, h, w')$ , leading to overlapping assignments. It is crucial to ensure that the final value of  $I'$  at any pixel  $(b, c, h, w')$  corresponds to the last assignment in the original processing order, consistent with the behavior of the nested loops.

**Baseline Implementation** The traditional implementation uses three nested loops over the batch, height, and width dimensions:

```
for batch in range(B):
    for row in range(H):
        for col in range(W):
            col_d = col + D[
                batch, 0, row, col] ** alpha * s
            if 0 <= col_d < W:
                I_prime[batch, :, row, col_d] =
                    I[batch, :, row, col]
```

This approach ensures correct handling of overlapping assignments by processing pixels in a specific order (e.g., from right to left when  $s \geq 0$ ) and overwriting previous values as needed. However, it is computationally inefficient due to the explicit loops.

**Proposed Vectorization Technique** Our method eliminates the explicit loops by vectorizing operations across the batch,

height, and width dimensions using PyTorch tensors. The key challenge is to replicate the assignment order of the nested loops to correctly handle overlapping assignments. First, we create tensors representing the batch, row, and column indices for all pixels. For positive movement such as  $s \geq 0$ , we process columns from right to left ( $W - 1$  to  $0$ ), while we process columns from left to right ( $0$  to  $W - 1$ ) for  $s < 0$ . For each column indices  $col$ , we then compute the offset  $D$  for each pixel and calculate the destination column indices  $col_d = col + D$ . Next, a Boolean mask is applied to filter out indices where  $col_d$  is outside the image boundaries. Note that the order for all valid indices is reversed to prioritize the last assignments in the original loop order. This conditional reversal ensures that, when duplicates are removed, the last assignment in the original loop order is preserved, correctly handling overlapping assignments. Next, we compute unique destination indices and keep the first occurrence, which corresponds to the last assignment due to reversal. We can then simply apply the computed index map to assign all pixels in bulk.

**Experimental Validation** We validate our method by comparing the outputs and execution times of the original and vectorized implementations, as shown in Table 3. The values are computed with 20 executions for each run. The results show that our implementation offers an effective solution for efficiently implementing pixel-wise image transformations that involve displacement based on depth maps or optical flow fields.

Resolution	128 × 128	512 × 512
Baseline (s)	1.48	23.3910
Ours (s)	0.0456	0.0116

Table 3. Performance evaluation of our vectorized method for displacement handling. Our implementation speeds up the operation for 936 and 2022 times for the image resolution of 128 and 512, respectively.

### B. Additional Experiments

We present additional experiment to further demonstrate the usability and validity of our proposed method.

#### B.1. Frame Interpolation And Looped Videos

Our method can be adapted to different video generation methods. We demonstrate generating stereo videos by using 1) frame interpolation, which generates stereo videos with a starting frame and an ending frame, and 2) looped videos, which generate a stereo video that keeps repeating without

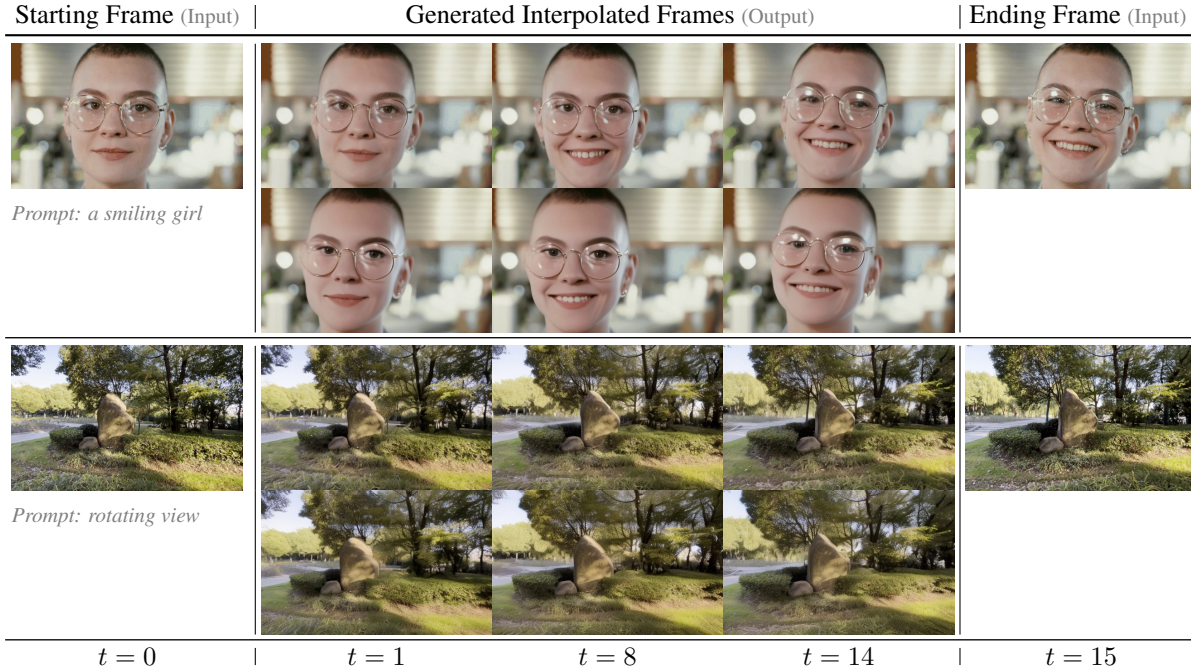


Figure 9. Demonstration of generating stereo videos with interpolated inputs. We input the starting and ending frames as our input and generate stereo content with our method. For each example, top row is the left view and bottom row is the right view.

breaking the continuity. We present our generated videos in Figures 9 and 10. This video generation process operates under a stricter condition, wherein only the required frames are fixed, while all other frames are initialized to zeros. Our approach follows a similar configuration as outlined in the main text. In addition, once the results are obtained, we remove the fixed frame indices because such hard constraints can disrupt the smoothness and natural continuity of the generated videos. From our experiments, we observe that those hard constraints eliminate the stereoscopic effects on those frames. This step ensures a more coherent and visually appealing video output while adhering to the imposed frame constraints during the generation process.

## B.2. Failure Cases

The failure cases of our method can be categorized into two scenarios: 1) the diffusion model failed to generate meaningful videos from the provided conditions, and 2) the generated target view image does not align with the source view. Since the first scenario depends on the choices of the diffusion model, we only discuss the second scenario in this section. In general, our method may fail when a small object moves with a strong motion. If the small object moves fast, the generated depth map may change rapidly while it may mess up the semantics of the latent space by the unnecessary intricate warping, resulting in a wrong interpretation of the depth and semantic information, as shown in Figure 11.



Figure 10. Demonstration of generating looped stereo videos. Starting with a single reference image, we produce a stereo video clip that seamlessly loops, offering visually continuous playback.

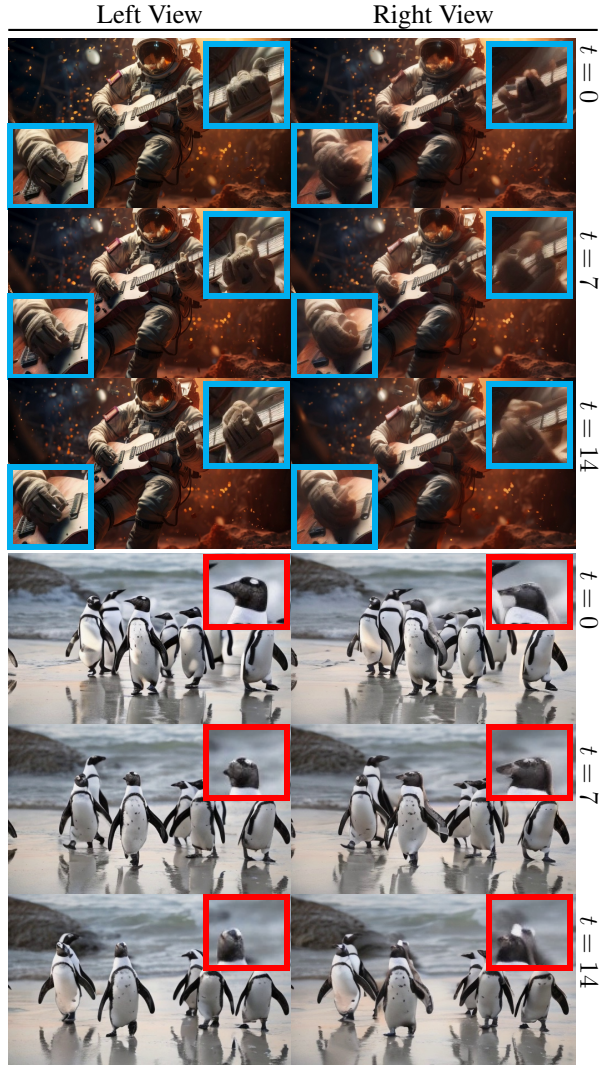


Figure 11. Demonstration of the failure cases. Our method can fail on the strong motion areas such as the rapid moving hand gesture and head pose.

### B.3. Multi-Resolution Support

Our method supports various resolutions, such as  $576 \times 1024$ ,  $320 \times 512$ , and  $256 \times 256$ . The images shown in our main text and supplementary materials are  $576 \times 1024$  and  $320 \times 512$  samples. In addition, we show  $256 \times 256$  samples in Figure 12 for demonstration purposes.

### B.4. A Pitfall in Latent Video Diffusion Models

Our method can be extended to other diffusion-based models. However, whilst experimenting with the naive latent video diffusion models (LVDMs), we found LVDMs can not handle repetitive patterns in the latent space properly. This can happen when inpainting the warped latent features with the source view latent. To further demonstrate that, we

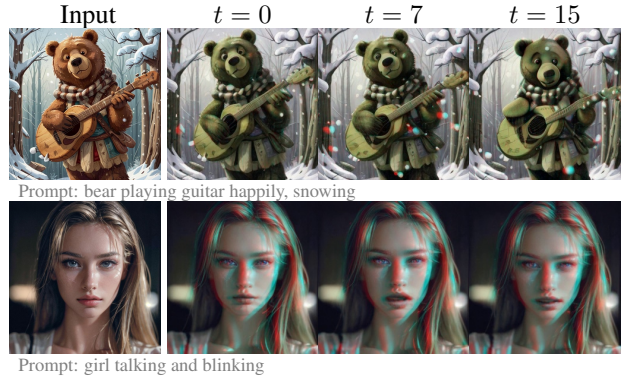


Figure 12. Demonstration of  $256 \times 256$  examples. Shown in anaglyph for visualizing the stereoscopic effect.

experiment by applying affine transformation (*s.t.* translation) to the latent space with border padding. We can observe that the generated images are degenerated, as shown in Figure 13.

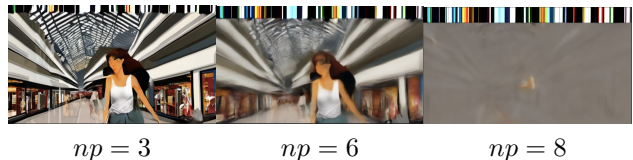


Figure 13. Warp LVDM latent space with direct translation with border padding on  $t = 10$ .  $np$  denotes the number of rows of pixels that are shifted.

In our experiment, such an issue can be avoided by avoiding the potential repetitive patterns, by inpainting with random Gaussian noises, or by our proposed noisy restart method (that uses both the source view latent and a small amount of random Gaussian noises). We show the improved results in Figure 14.

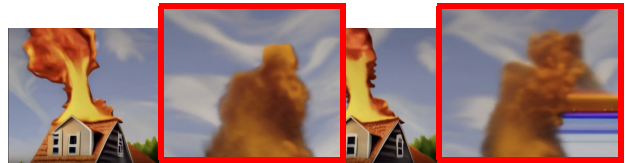


Figure 14. Demo of repetitive latent warping for LVDMs. Left: filling with source view (w/o repetitive patterns). Right: filling with random noise (w/ repetitive patterns).

## C. Perfect Depth Maps Can Be Imperfect

This section introduces a disparity propagation approach that can generate depth maps with consistent depth values, then we compare this solution against the video depth estimation approach.

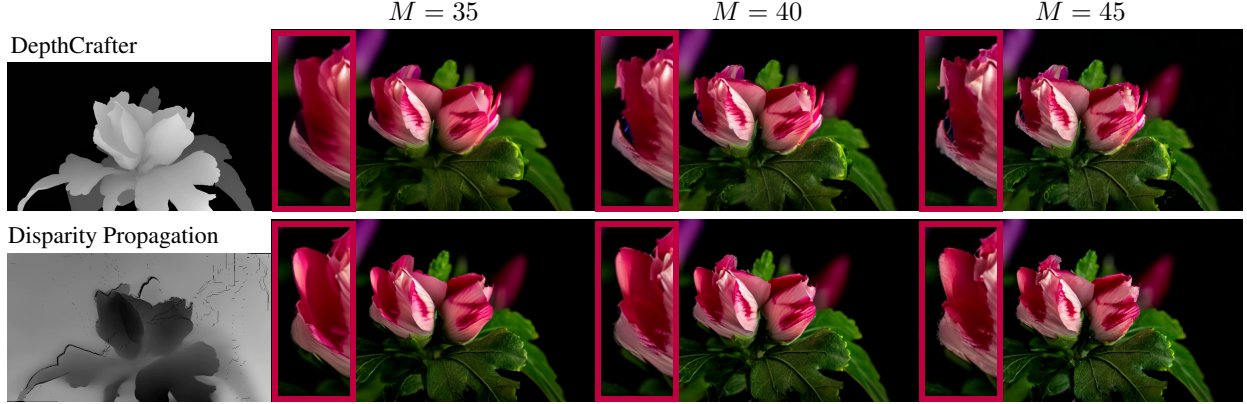


Figure 15. Demonstration of the differences between using DepthCrafter and Disparity Propagation method for obtaining disparity values.  $M$  denotes the early-stop sampling step for the warping operation. Both depth images and generated samples are taken from the 12<sup>th</sup> frame. We can see that DepthCrafter offers a better depth map but it may create sharp textures for a larger  $M$  while the disparity propagation method may mitigate such effects though a less accurate depth map provided.

### C.1. Disparity Propagation

With an aim of a more stable video with fewer artifacts, we first obtain a video depth map that allows smoother transitions and minimizes abrupt depth changes. Therefore, we propose *disparity propagation*, that propagates depth information from a single, initial depth frame across the entire video using frame-by-frame optical flow warping. This approach provides a smoother, more consistent disparity map over time, as it mitigates frame-specific artifacts by avoiding the per-frame recalculation of depth.

Given an initial depth map  $D_t$  for the frame at time  $t$ , we estimate the depth map at the previous  $t + 1$  frame and the next  $t - 1$  frame by warping  $D_t$  based on the forward and backward optical flow,  $F_{t \rightarrow t+1}$  and  $F_{t \rightarrow t-1}$ . We use a warping operation to apply the optical flow  $F_{t \rightarrow t+1}$  to adjust  $D_t$  based on the motion between the frames. The forward warping function can be expressed as:

$$D_{t+1}(x, y) = D_t(x + F_{t \rightarrow t+1}^x(x, y), y + F_{t \rightarrow t+1}^y(x, y)). \quad (12)$$

Note that the backward warping  $D_t$  to  $D_{t-1}$  can also be achieved with this operation since  $F_{t+1 \rightarrow t} = -F_{t \rightarrow t+1}$ . We repeat the process for each precedent and subsequent frame to propagate the initial depth across the entire video sequence. This produces a sequence of disparity maps  $\{D_0, D_1, \dots, D_T\}$  that are inherently smooth and consistent over time.

### C.2. Disparity Propagation vs. Video Depth Estimation

Existing video depth estimation models often overemphasize subtle scene movements, such as the drift of particles or minor background elements. Commonly, such objects are fine-grained high-frequency information that is not ex-

hibited in the early stages of a diffusion latent representation. As shown in Figure 16, the early latent spaces mostly emphasize the low-frequency structure information. The di-

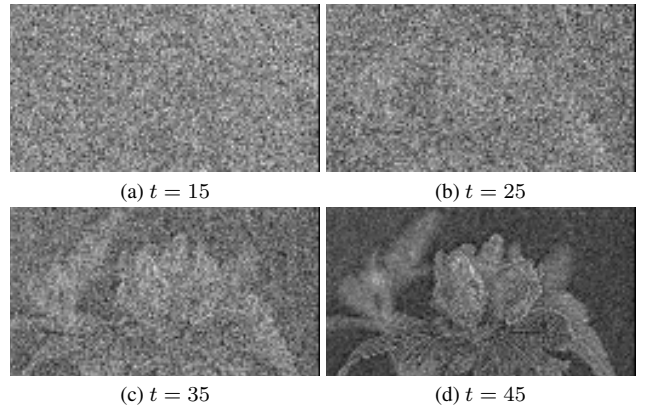


Figure 16. We visualize the tensor of the first timeframe in the first channel of the latent space of video diffusion. We can observe that the significant structural information does not show before  $t = 25$ .

rect use of video depth estimation results may mistakenly warp the low-frequency latent component using the prediction of high-frequency depth maps. This can lead the model to assign high importance to irrelevant objects or minor details, which misleads the generation model into emphasizing non-crucial elements. Moreover, although these models generally produce consistent depth estimates across the scene, they occasionally introduce significant artifacts. For instance, objects may appear to shift abruptly from far to near within the frame, or objects ignored in previous frames may suddenly appear, leading to sudden jumps in perceived depth. Such inconsistencies can result in collapsed or distorted video generation. As shown in Figure 15, the depth

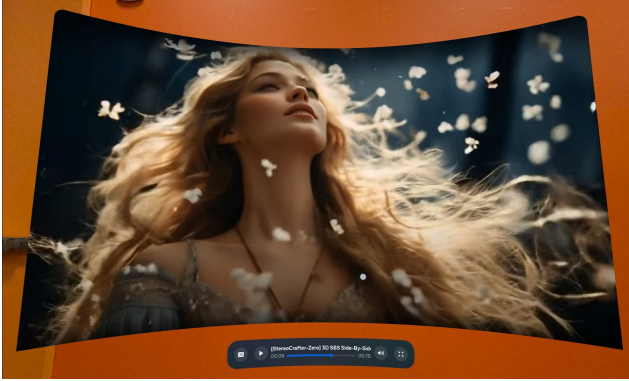


Figure 17. A screenshot captured on Meta Quest 3, showcasing a 3D movie in action.

map generated from a video depth estimator may mess up the border values due to the potential inconsistency around the edges, which is especially crucial for warping since the values may be moved to a wrong location.

In our current implementation, we still prefer a video depth estimator since this depth propagation approach may fail to generate a meaningful disparity map to handle the scenarios that come with a strong motion. However, supported by our aforementioned experiment, one potential solution might be employing a progressive depth map that can gradually increase the depth information for high-frequency objects. In the future, we believe a progressive depth map may further benefit the generation process.

## D. User Study

Our survey is designed with four questions for each method, such as:

1. *Frame Quality (5 is best, 1 is poor)*
2. *Temporal Coherence (5 is best, 1 is poor)*
3. *Stereoscopic Effects (5 is best, 1 is poor)*
4. *Overall Conformity (5 is best, 1 is poor)*

The answer for each question is a radio of five integer values ranging from 1 to 5. Then each participant would watch our prepared videos on a Meta Quest 3 device. Figure 17 showcases a 3D movie being viewed through the headset. The study included 2 users who reported previous difficulty with 3D effects and 5 users who came with previous VR headset experiences.